A physics-informed deep learning approach for bearing fault detection

Sheng Shen [a,1], Hao Lu [a,b], Mohammadkazem Sadoughi [a,2], Chao Hu [a,b,*], Venkat Nemani [a],
Adam Thelen [a], Keith Webster [c], Matthew Darr [c], Jeff Sidon [d], Shawn Kenny [e]

[a] *Department of Mechanical Engineering, Iowa State University, Ames, IA 50011, USA*
[b] *Department of Electrical and Computer Engineering, Iowa State University, Ames, IA 50011, USA*
[c] *Department of Agricultural and Biosystems Engineering, Iowa State University, Ames, IA 50011, USA*
[d] *John Deere Intelligent Solutions Group, Johnston, IA 50023, USA*
[e] *John Deere Des Moines Works, Ankeny, IA 50023, USA*

ARTICLE INFO

ABSTRACT

In recent years, advances in computer technology and the emergence of big data have enabled deep learning to achieve impressive successes in bearing condition monitoring and fault detection. While existing deep learning approaches are able to efficiently detect and classify bearing faults, most of these approaches depend exclusively on data and do not incorporate physical knowledge into the learning and prediction processes—or more importantly, embed the physical knowledge of bearing faults into the model training process, which makes the model physically meaningful. To address this challenge, we propose a physics-informed deep learning approach that consists of a simple threshold model and a deep convolutional neural network (CNN) model for bearing fault detection. In the proposed physics-informed deep learning approach, the threshold model first assesses the health classes of bearings based on known physics of bearing faults. Then, the CNN model automatically extracts high-level characteristic features from the input data and makes full use of these features to predict the health class of a bearing. We designed a loss function for training and validating the CNN model that selectively amplifies the effect of the physical knowledge assimilated by the threshold model when embedding this knowledge into the CNN model. The proposed physics-informed deep learning approach was validated using (1) data from 18 bearings on an agricultural machine operating in the field, and (2) data from bearings on a laboratory test stand in the Case Western Reserve University (CWRU) Bearing Data Center.

1. Introduction

Modern machinery is becoming increasingly complex, while the operating conditions are typically harsh and uncertain, which increases system vulnerability and eventually leads to a breakdown. An unanticipated machine failure requires unplanned maintenance, and maintenance delays often affect other related components in the system. Monitoring the health condition of a machine can help increase machine availability, reduce the cost of downtime, and improve customer satisfaction (Kang et al., 2016). Rolling element bearings are not only the most critical components but also the main contributors to system failures; 45%–55% of rotating machine failures are caused by rolling element bearing failures (Kang et al., 2016; Lanham, 2002; Nandi et al., 2005). Therefore, detecting bearing faults is a major concern and has drawn substantial research attention. According to the current literature, a general intelligent fault detection methodology includes three steps: data acquisition, feature extraction, and fault classification (Hoang and Kang, 2019).

The data acquisition step acquires signals that reflect bearing health conditions. Various sensing techniques, including vibration (Saufi et al., 2019; Lei et al., 2016; Dolenc et al., 2016; Abboud et al., 2019), acoustic emission (Hasan et al., 2019; Van Hecke et al., 2016; Glowacz, 2019), and motor current (Soualhi et al., 2019; Azamfar et al., 2020; Singh and Kumar, 2016), have been applied to bearing health monitoring and fault detection. Vibration sensors are commonly used due to their widespread availability and sensitivity in bearing fault detection (Cerrada et al., 2018). The discussion in the remainder of this paper will be confined to vibration-based health monitoring.

The feature extraction step maps the original signals onto statistical parameters that convey machine status information. The design of the feature extractor plays a very important role in obtaining high accuracy. Feature extraction methods can be divided into two types: physics-based methods and data-driven methods. For physics-based methods, signal features can be extracted from the time domain (Cerrada et al., 2018), frequency domain (Sikder et al., 2019), and time–frequency domain (Liu et al., 2016). The original vibration signals

collected from rotating machines are almost always in the time domain; however, for bearing fault detection, these vibration signals are often investigated in the frequency domain and the time–frequency domain by using the appropriate tools to transform raw time-domain signals into the corresponding domains. The Fourier transform is the most popular signal processing tool used to transform a vibration signal into the frequency domain (Seryasat et al., 2010). Time–frequency domain features can be extracted by the wavelet packet transform (Wang et al., 2015), Morlet wavelet transform (Tang et al., 2010), and short-time Fourier transform (Liu et al., 2016). The data-driven feature extraction relies on the use of machine learning models to automatically learn the most informative features from the raw data (Rai and Upadhyay, 2016; Jia et al., 2016; Abdeljaber et al., 2017; Vincent et al., 2010; Pan et al., 2016). Jia et al. (2016) proposed a deep learning-based method to mine the useful information from raw data and approximate complex nonlinear relationships between collected signals and the health condition of bearings and achieved satisfactory fault detection accuracy under various operating conditions. Lei et al. (2016) proposed a sparse filtering-based deep neural network to directly learn features from mechanical vibration signals. Abdeljaber et al. (2017) proposed 1D CNN on a normalized vibration signal, which can perform vibration-based damage detection and localization of the structural damage in real-time.

After the features are extracted, they are input into the fault detection model to estimate the health condition of the machine. Several machine learning-based models can be utilized to achieve bearing fault detection, such as k-nearest neighbors (Cover and Hart, 1967; Tian et al., 2015), artificial neural network (Sadeghian et al., 2009; Schmidhuber, 2015), support vector machine (Cortes and Vapnik, 1995; Banerjee and Das, 2012), and Bayesian networks (Cai et al., 2016b,a). Tian et al. (2015) formed a health index using principal component analysis and k-nearest neighbors to detect bearing faults and monitor the degradation of bearings. Sadeghian et al. (2009) presented an approach for induction motors online detection of rotor bar breakage, based on the combination of wavelet packet decomposition and an artificial neural network. Banerjee and Das (2012) investigated a hybrid method for fault signal classification based on sensor data fusion by using a support vector machine and short-time Fourier transform techniques. Cai et al. (2016b) proposed a two-layer dynamic Bayesian networks-based approach to detecting faults of electronic systems. The second fault symptom layer was used to detect system faults after receiving the fault information from the first fault layer. To reduce the overall complexities of Bayesian networks in fault diagnosis, Cai et al. (2016a) proposed an approach using object-oriented Bayesian networks for the real-time fault diagnosis of a subsea production system. Dou and Zhou (2016) compared the bearing fault detection results of k-nearest neighbors, a probabilistic neural network, a particle swarm optimization optimized support vector machine, and a rule-based method. Although these shallow machine learning-based models are able to produce satisfactory accuracy in bearing fault detection, they lack the capability to analyze and derive full value from large volumes of data (Lei et al., 2020).

In recent years, deep learning has attracted increasing attention from researchers in the field of bearing fault detection and has additionally been recognized as a powerful tool for bearing failure prognosis (Jin et al., 2019; Zhao et al., 2019; Rai and Upadhyay, 2018; Ahmad et al., 2017; Wang et al., 2016; Li et al., 2016). Deep learning models can automatically extract complex features from the input data without requiring human intervention. Three deep learning architectures are widely used for bearing fault detection: the autoencoder (Lu et al., 2017; He et al., 2016), restricted Boltzmann machine (Xing et al., 2017), CNN (Eren et al., 2019; Jing et al., 2017; Zhang et al., 2018; Khorram and Khalooei, 2019; Kim and Youn, 2019), and their variants. He et al. (2016) proposed a novel loss function for increasing the robustness of an autoencoder in bearing fault detection. Xing et al. (2017) developed a locally connected restricted Boltzmann machine to address

the periodic appearance of fault features in the raw signals. Then, based on the features learned by the restricted Boltzmann machine, they used softmax regression to recognize faults. Recently, CNNs have attracted attention from researchers in the machinery fault detection field (Eren et al., 2019). A CNN has a feed-forward architecture consisting of two fundamental operators: convolution and pooling. The convolution operator extracts local features from the input using various filters (also known as kernels). The pooling operator extracts features with a fixed-length over sliding windows of the input data following several rules, such as averaging and maximizing. One unique characteristic of a CNN is that it can automatically extract high-level characteristic features from large volumes of data and thus avoid the manual feature extraction that relies heavily on human labor. Jing et al. (2017) proposed a CNN-based feature learning and fault detection model for fault detection of a gearbox and compared the model performance with three machine learning methods. The comparison results showed that the proposed CNN model achieved the best performance on different data types. To improve the robustness of CNNs in bearing fault detection, Zhang et al. (2018) proposed a CNN with training interference that enabled the model to detect bearing faults with input noisy data collected from different working conditions.

Although many deep learning models have recently been implemented and applied to monitor the health of rolling element bearings, little research effort has been devoted to incorporating physical knowledge into deep learning methods—or more importantly, seek ways to incorporate the physical knowledge of bearing faults into the model training process to make model physically meaningful and applicable in different application scenarios. Compared to a purely data-driven model, a physics-informed deep learning model emphasizes the features that carry the most useful bearing fault-relevant information. By leveraging domain knowledge, physics-informed deep learning models can alleviate the number of misclassifications that are contrary to physics (such as a false positive that occurs when a model incorrectly predicts a bearing fault while the vibration amplitudes at all frequencies take very small values). Mohammad et al. developed a deep CNN model that was equipped with a physics-based convolutional layer as the first layer for bearing fault detection (Sadoughi and Hu, 2019). Subsequently, Lu et al. attempted to improve the performance of this deep CNN model by proposing a physics-based feature-weighting technique (Lu et al., 2019) that could flexibly optimize how physical knowledge is incorporated in the frequency domain.

Moreover, most of the existing bearing fault detection approaches are dependent on data collected from laboratory test stands. However, in many real-world applications, the data are often collected in more complex and variable working conditions (such as rotating speeds, loads, etc.). The existing approaches thus may not perform well in these real-world scenarios. In this work, we aim to develop and validate a physics-informed deep learning approach based on the data collected from an agricultural machine operating in the field. The contribution of our work is four-fold.

First, a novel deep learning approach called physics-informed deep learning is proposed for bearing fault detection. The proposed approach has the ability to leverage the physical knowledge of bearing faults to ensure satisfactory detection accuracy under highly time-varying rotational speeds. Compared to purely data-driven approaches which do not incorporate physical knowledge into the learning process, the proposed approach produces a higher level of compliance with physics, thereby improving the learning model's credibility.

Second, we define nine frequency sub-bands centering around the bearing fault characteristic frequencies and use the vibration amplitude readings in the sub-bands as the input features. Our rationale is that the readings in these sub-bands may carry more fault-relevant information than the readings in other frequency sub-bands. These input features, which are selected based on the physical knowledge of bearing faults, may improve the ability of a deep learning model to learn highly representative features for bearing fault detection.

Third, a customized data-and-physics-driven loss function is designed to intelligently incorporate the physical knowledge of fault-relevant information into the deep learning model training process, making the model physically meaningful.

Fourth, the proposed physics-informed deep learning approach is validated using bearing data collected from a heavy-duty off-road vehicle used for an agricultural application (Case Study 1) and from a laboratory test stand in the Case Western Reserve University (CWRU) Bearing Data Center (Case Study 2).

The remainder of this paper is organized as follows. Section 2 provides background information, including bearing fault characteristic frequencies and signal preprocessing techniques. Section 3 discusses the selection of the input sub-band envelope spectrum, and the development of a customized data-and-physics-driven loss function to integrate the physical knowledge from the threshold model with the data-driven CNN for bearing fault detection. Section 4 introduces the experimental data used to verify the proposed physics-informed deep learning approach. The fault detection results by the proposed approach and other data-driven approaches are reported in Section 5, and concluding remarks are presented in Section 6.

2. Background

2.1. Fault characteristic frequencies

Bearings are composed of four main components: the inner race, outer race, rollers or balls, and the cage. The periodic frequency caused by a bearing fault is called the fault characteristic frequency, which can be uniquely determined by the location of the fault, the shaft frequency, and the geometric parameters of the bearing (Sadoughi and Hu, 2019; Lu et al., 2019; Zhang et al., 2017). In this study, we consider three main types of bearing faults: inner race fault, outer race fault, and roller or ball fault. The fault characteristic frequency formulae of these three types of bearing faults are as follows:

$$f_{IRD} = f_r \times \frac{Z}{2}(1 + \frac{d}{D}\cos\alpha) \tag{1}$$

$$f_{ORD} = f_r \times \frac{Z}{2}(1 - \frac{d}{D}\cos\alpha) \tag{2}$$

$$f_{RD} = f_r \times \frac{D}{2d}\left\{1 - \left(\frac{d}{D}\right)^2\cos^2\alpha\right\} \tag{3}$$

where d is the roller or ball diameter ball, D is the pitch diameter, f_{IRD}, f_{ORD}, and f_{RD} denote the fault characteristic frequencies of the inner race, outer race, and rolling element, respectively, Z denotes the number of rollers or balls, f_r denotes the shaft rotational frequency, and α denotes the angle of the load from the radial plane.

2.2. Signal preprocessing

When a bearing has a localized fault, contact between the fault and its mating surface excites a periodic impulse response with a frequency called the fault characteristic frequency. The vibration signal in the presence of this fault exhibits an amplitude modulation phenomenon that combines the characteristic frequency of the bearing fault with the structural resonance of the host system. Due to the modulation, a high energy resonance frequency band is formed around the system resonance frequency. By contrast, the energy in the signal spectrum's low-frequency band (where the fault characteristic frequency and its first few harmonics are located) is extremely weak. This makes it difficult to analyze the fault characteristic frequencies directly from the frequency spectrum. To tackle this difficulty, demodulation techniques have been developed that extract the fault-related vibration component from the modulated signal. Envelope analysis, also known as amplitude demodulation, is a well-known demodulation technique for bearing vibration analysis (Cheng et al., 2014). One method of envelope analysis is to first apply a bandpass filter and then use a Hilbert transform. The purposes of the bandpass filter are to remove the low-frequency high-amplitude signals associated with imbalance and misalignment and to eliminate random noise outside the passband. After the bandpass filter is applied, the Hilbert transform is used to rectify the filtered signal.

The Hilbert transform is a signal demodulation technique that can reveal fault information by constructing an analytical signal from a sample vibration signal. An analytical signal is a complex time-domain signal whose imaginary component is the Hilbert transform of the real part. Thus, if $a(t)$ denotes the time-domain signal and $H(a(t))$ denotes its Hilbert transform, the analytical signal can be defined as $A(t) = a(t) + jH(a(t))$, where j denotes the unit imaginary number. It can be proven that the Hilbert transform corresponds to a 90° phase shift in the time domain (Feldman, 2011). By using the Hilbert transform, rapid oscillations can be removed from the modulated signal to produce a direct representation of the fault characteristic frequencies (Randall and Antoni, 2011).

A sample vibration signal in the presence of an outer race fault is shown in Fig. 1. It can be seen that the modulated signal contains little to no diagnostic information about bearing faults in both the time domain (the blue waveform in Fig. 1(a)) and frequency domain (the blue spectrum in Fig. 1(b)). The red dashed waveform in Fig. 1(a) shows the enveloped signal, demodulated using the Hilbert transform. From the red spectrum in Fig. 1(b), it can be seen that the spectrum of the signal envelope reveals useful information for fault diagnosis, such as the fault characteristic frequency (f_{ord}), its first harmonic ($2 \times f_{ord}$), and potential modulations.

As shown in Eqs. (1) to (3), each fault characteristic frequency is the product of a constant value and the shaft speed. The computed order tracking technique is applied to eliminate the frequency shift caused by speed change. Instead of sampling the signal at constant increments of time, the computed order tracking technique samples the vibration signal at constant increments in the shaft angle. After performing computed order tracking and envelope analysis, the vibration signal can be converted from a time series signal to an enveloped order spectrum. The order is defined as the frequency normalized by the reference speed and takes the following form (Fyfe and Munck, 1997)

$$o = f/f_r, \tag{4}$$

where o denotes the order, f denotes the frequency of the observed vibration, and f_r denotes the reference speed, which is set as the shaft's rotational speed. A more detailed description of computed order tracking can be found in Cheng et al. (2014).

2.3. Physics-informed deep learning

During the past few years, deep learning has been recognized as a useful tool in bearing condition monitoring and fault detection. Most of the deep learning approaches rely exclusively on data and do not incorporate physical knowledge into the learning and prediction processes. Without incorporating physical knowledge, purely data-driven approaches may have a low level of compliance with physics, leading to poor model performance. In Fig. 2, we show the level of compliance versus the overall accuracy for three approaches in Case Study 1 (will be detailed later). A lower level of compliance with physics means a larger percentage of misclassifications that are also contrary to physics, which often leads to a lower level of the learning model's credibility. By leveraging physical knowledge of bearing faults, a physics-informed deep learning approach can reduce the number of misclassifications that are incompliant with physics, thereby improving the model's credibility.

3. Methodology

3.1. Input feature extraction and output fault detection

The objective of this study is to detect bearing faults using the sub-band envelope spectra of vibration signals; which are considered
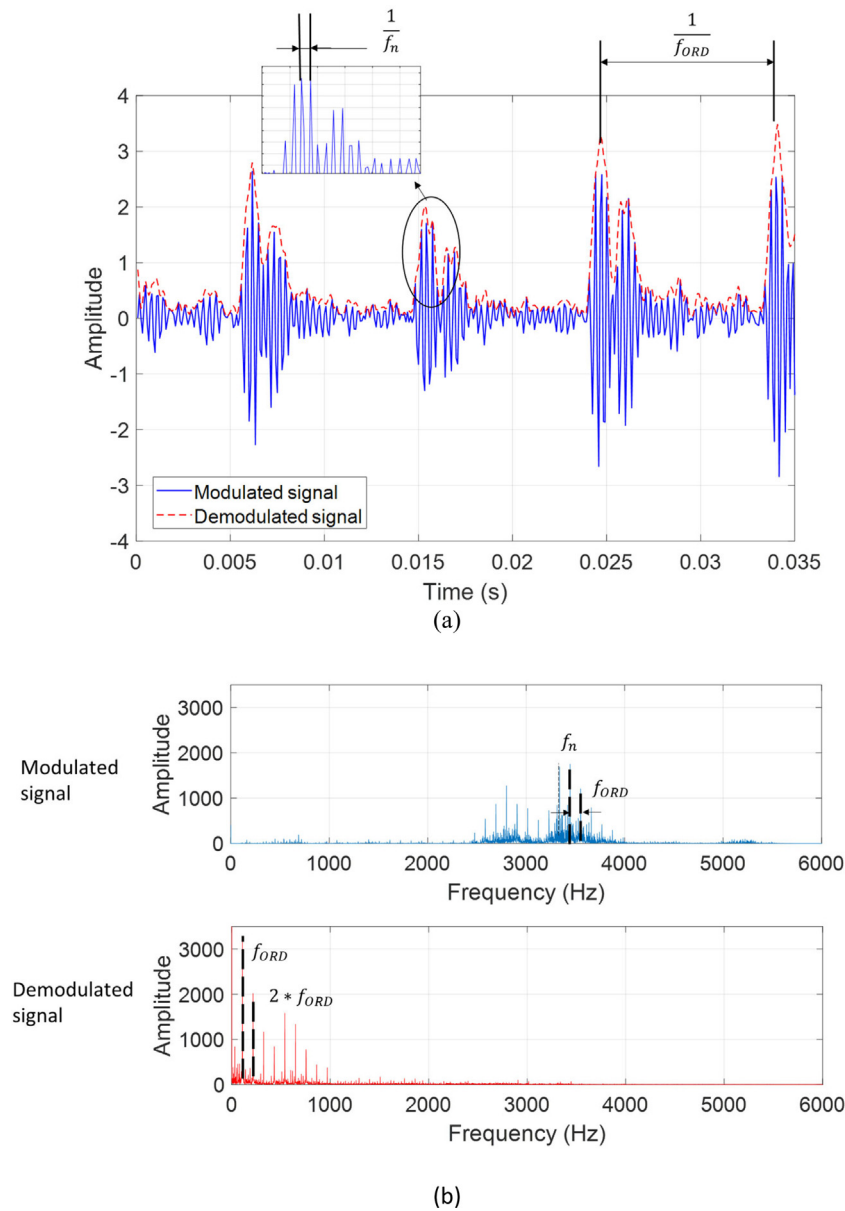
Fig. 1. Bearing vibration signals in the presence of an outer race fault: (a) time-domain signal and (b) frequency-domain signal.

to be the input features used by the proposed physics-informed deep learning approach. The sub-band envelope spectrum is obtained via two steps: (1) analyze the raw time-domain vibration signal with a sampling rate of 25,600 Hz using the Hilbert transform, fast Fourier transform (FFT), and computed order tracking to obtain its envelope signal in the frequency domain ranging from order 0–34; and (2) select the frequency sub-bands based on the fault characteristic frequencies of the bearing, as shown in Fig. 3 (for Case Study 1).

Instead of using the entire envelope spectrum as input features for bearing fault detection, we only select the frequency sub-bands in the envelope spectrum according to the fault characteristic frequencies, due to the following reasons. First, the centers of the sub-bands for each fault type correspond to the characteristic fault frequency and its harmonics. As described in Section 2.2, a fault characteristic frequency is the frequency of periodic impulses triggered by a bearing fault and the fault characteristic frequencies can be treated as known physics of bearing faults. The design of the learning-model input in the proposed approach is thus informed by the physics of bearing faults. Second, the center frequencies are symmetrically extended in both directions by 5% of the center frequency values to form these sub-bands. This percentage

value is determined according to the model's performance on the validation set (see Section 5.1.4). The narrow frequency bands centered around the fault characteristic frequencies and their harmonics are selected as the sub-bands because the vibration amplitudes within these frequency bands potentially carry more fault-relevant information than those at frequencies outside these bands. Third, there could be a potential offset in the calculation of the characteristic frequency due to the bearing dimensional tolerances and/or the resolution bias error in the frequency spectrum (picket-fence effect) (Tsao et al., 2001). Thus, using a frequency range instead of a single frequency value may allow for enough margin to accommodate these errors. Note that the deep learning models in both Case Study 1 and Case Study 2 take the respective sub-band envelope spectra as the input features. The fault detection results of these two case studies are presented in Sections 5.1 and 5.2, respectively.

The selection of appropriate sub-bands is essential for effective fault diagnosis, as it can reveal intrinsically explicit information about different types of bearing faults. Table 1 summarizes the order ranges of nine selected sub-bands, defined using the fault characteristic frequency f_c and sub-band width (%) n. As mentioned in Section 2.1, the fault
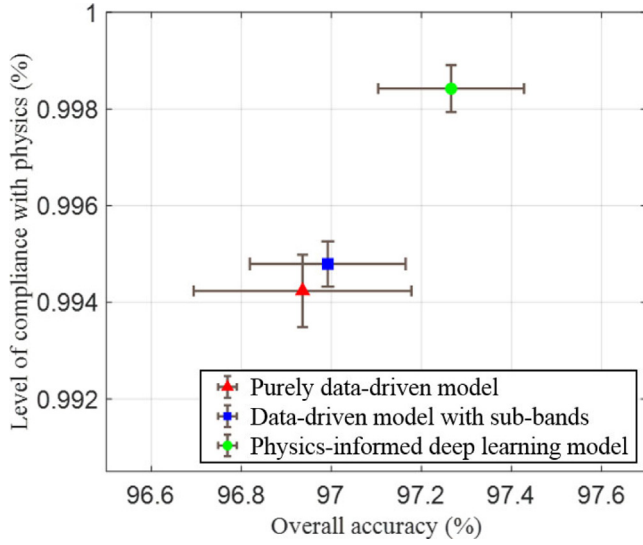
Fig. 2. Level of compliance with physics vs. overall accuracy for different approaches used in Case study 1. The error bars indicate ± one standard deviation.
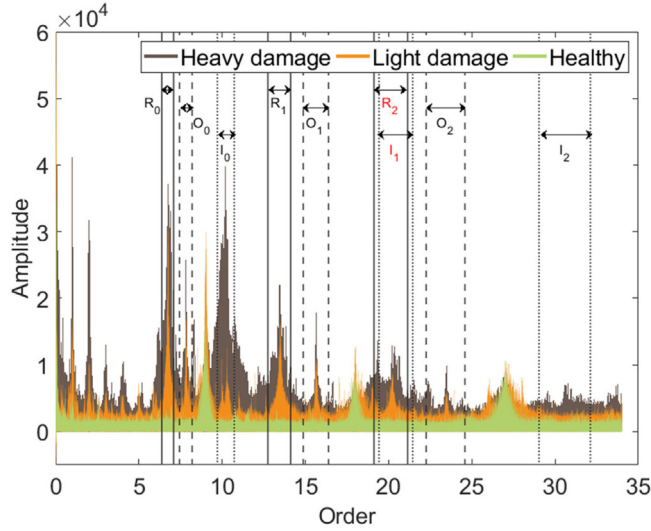

Fig. 3. An illustration of the selected frequency sub-bands. R_{0-2}, O_{0-2}, and I_{0-2} denote the bearing sub-band order range in the characteristic frequency and its first two harmonics for the roller fault, outer race fault, and inner race fault, respectively. Note that R_2 and I_1 have the overlapped ranges and that the bearings used in Case Study 1 are roller bearings.

characteristic frequencies of inner race, outer race, and roller can be calculated based on the geometry of the bearing, according to Eqs. (1)–(3). Thus, the order ranges of the sub-bands for each fault type have their centers located at the fault characteristic frequency (f_c) and its first two harmonics and their widths defined as a certain percentage (n) of the sub-band central frequency, extending symmetrically in both directions. After identifying the order ranges of the nine sub-bands using f_c and n (i.e., $f_c(1 \pm n)$), the characteristic features localized in the order ranges, which contain explicit information associated with the roller, outer race, and inner race faults, are chosen for bearing fault detection. We note that the order ranges shown in Table 1 are for Case Study 1 and will vary for a different bearing.

Each vector of input features (i.e., the sub-band envelope spectrum) has a corresponding health class that serves as the ground truth of a bearing's health class. This study aims to detect the degree of bearing degradation instead of distinguishing the types of bearing faults. The

model output (or fault detection result) in this study, is, therefore, one of three health classes, namely, healthy, light damage, and heavy damage, that represent three distinct levels of bearing degradation.

3.2. Overall methodology of physics-informed deep learning

This study seeks to create a physics-informed deep learning approach for bearing fault detection. This approach involves the use of a threshold model and a deep CNN model.

The threshold model is a straightforward method that determines the health class of a bearing based on two thresholds, termed threshold 1 and threshold 2, which are identified by the highest amplitudes of the envelope spectrum in the training dataset, as shown in Fig. 4. Fig. 4 shows the selected sub-band envelope spectra for the training dataset used in this study. The value of threshold 1 (i.e., 2800) is selected based on the highest amplitude among the envelope spectra of the bearings in the healthy class (i.e., green spectra); the value of threshold 2 (i.e., 31,000) is determined based on the highest amplitude among the envelope spectra of the bearings with light damage (i.e., the orange spectra). Although the value of threshold 1 is much lower than that of threshold 2, it is expected that the vibration of a healthy bearing shows significantly lower amplitudes on the envelope spectrum than that of a faulty bearing. Because of the way the value of threshold 1 is determined, the vibration amplitudes of a healthy bearing in the training dataset are unlikely to exceed this threshold. Therefore, the use of threshold 1 allows distinguishing healthy bearings from those with light damage and heavy damage and ensures a very low likelihood that healthy bearings are misclassified as those with light or heavy damage. Note that threshold 2 may be overestimated because some of the bearings with heavy damage may not have amplitudes above 31,000. While threshold 2 cannot distinguish all bearings with heavy damage from bearings with light damage, it is highly probable that heavy damage predictions made by this threshold model are correct due to the high amplitude of threshold 2. This assumption is important as this physical knowledge will be used to refine the possibly incorrect health classifications made by the CNN model. It is not surprising that the deep learning model does not generalize well to samples not encountered during training because this model is purely data-driven and cannot effectively discover and leverage information about bearing fault physics that is often hidden in the envelope signals. Thus, the threshold model can predict the bearing health classes based on fault-relevant information (i.e., thresholds 1 and 2) extracted from the envelope signals. It is worth mentioning that the values of threshold 1 and threshold 2 are empirically determined based on the fault information of the training data rather than the test data. In this study, neither threshold varies with the feature index or order. Alternatively, one may explore the use of a more complex threshold model where both thresholds vary with the feature index and order and are thus frequency-dependent. However, such an exploration is beyond the scope of this study.

The architecture of the CNN model used in this study is shown in Fig. 5. The CNN model consists of six building components, five of which are convolutional stages and the remaining one is a fully connected stage. Each convolution stage is composed of a convolutional layer, a batch normalization (BN) layer, and a rectified linear unit (ReLU) except for the first convolution stage, in which an additional max-pooling layer is applied to the ReLU output. The BN layer is designed to increase the robustness to CNN initialization and normalize its input across mini-batches to accelerate CNN training. This layer is usually added between the convolutional layer and the ReLU activation layer. ReLU is typically applied after the BN to enhance the network's ability to represent the nonlinearity of the input envelope signals. The fully connected stage follows the five convolution stages. In this stage, the extracted high-level features from the last convolution stage are flattened to a fixed-dimensional vector, which is then fully connected to the output layer to perform the health classification. Finally, a softmax layer computes the estimated probabilities for all the health classes and outputs the class with the highest probability.

Table 1

Summary of the sub-band envelope spectrum and the number of characteristic features. The sub-band width is set to 5% for the purpose of calculating the number of selected features. The predetermined rate of 5% is selected according to the target task performance on the validation set.

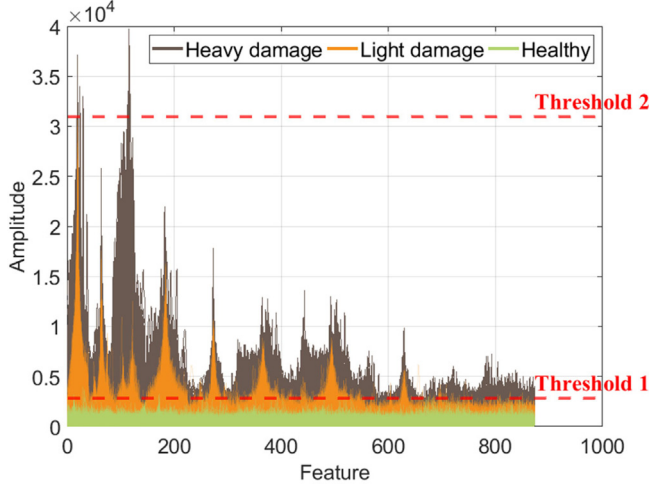| Item	Roller fault			Outer race fault			Inner race fault		
	R_0	R_1	R_2	O_0	O_1	O_2	I_0	I_1	I_2
Characteristic frequency, f_c	6.75			7.8			10.2		
Sub-band	$f_c(1 \pm n)$	$2f_c(1 \pm n)$	$3f_c(1 \pm n)$	$f_c(1 \pm n)$	$2f_c(1 \pm n)$	$3f_c(1 \pm n)$	$f_c(1 \pm n)$	$2f_c(1 \pm n)$	$3f_c(1 \pm n)$
Order range	[6.41,7.09]	[12.83,14.18]	[19.24,21.26]	[7.47,8.19]	[14.82,16.38]	[22.23,24.57]	[9.69,10.71]	[19.38,21.42]	[29.07,32.13]
Number of features	39	79	118	46	92	138	60	120	180

Fig. 4. Amplitude vs. feature for the eight bearings in the training dataset. Thresholds 1 and 2 are 2800 and 31,000, respectively.

The goal of this study is to bridge the gap between the sensor data and physical mechanisms by facilitating a tight integration of data-driven learning and physics-informed modeling. This integration is realized via a customized data-and-physics-driven loss function. Fig. 6 illustrates the application of a customized data-and-physics-driven loss function to the proposed physics-informed deep learning approach for bearing health classification.

The proposed approach embeds the physical knowledge from the threshold model into the model's training process by employing a customized data-and-physics-driven loss function. The model adds a penalty to the loss function when the predictions of the CNN and the threshold model disagree on the healthy and heavy damage classes. The penalty guides the model toward the known physical bearing fault knowledge from the threshold model that we believe is correct. More implementation details regarding the customized data-and-physics-driven loss function are presented in the following section.

3.3. Data-and-physics-driven loss function

The main idea behind the proposed physics-informed deep learning approach is to embed known fault-relevant knowledge as prior information in the neural network training process, building a physically meaningful deep learning model for bearing fault detection. This objective is achieved by employing a customized data-and-physics-driven loss function, $Loss_{DP}$:

$$Loss_{DP} = Loss_{all} + \alpha \cdot Loss_g + \beta \cdot Loss_r, \tag{5}$$

$$Loss_{all} = -\frac{1}{N} \sum_{j=1}^{N} \sum_{i=1}^{n} y_{ji}^T \log(\overline{y}_{ji}), \tag{6}$$

where $Loss_{all}$ denotes the traditional cross-entropy loss function for classification tasks, which measures the compatibility between a predicted bearing health class (e.g., the fault detection result) and its
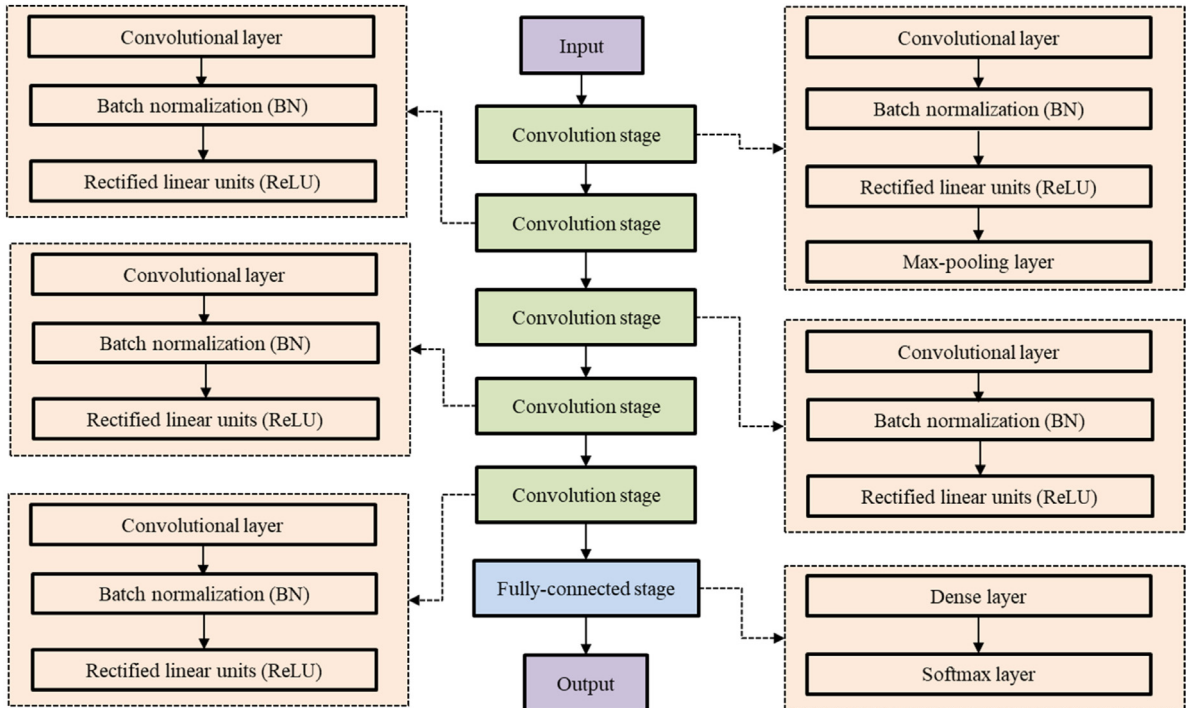

Fig. 5. Overview of the architecture of the CNN model used in this study (Shen et al., 2018, 2019a,b, 2020).
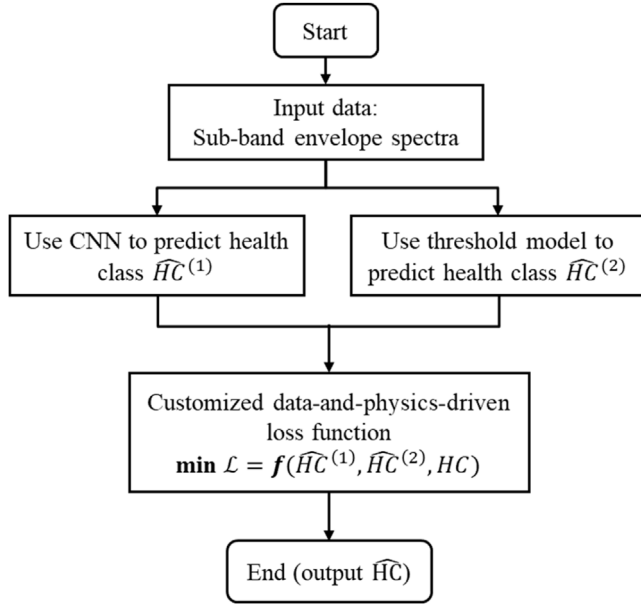
Fig. 6. Implementing the integration of data-driven learning and physics-informed modeling.

Table 2
List of parameters and their values during the training of the physics-informed deep learning model.

Parameter	Value
Initial learning rate	0.01
Mini-batch size	128
Momentum	0.9
L_2 Regularization	0.0005
Number of epochs	22

Table 3
Summary of the physics-informed deep learning model configurations. Conv-l and DC-l denote the lth convolutional layer and dense layer, respectively. For brevity, the BN layer and ReLU activation layer are not shown.

Layer name	Filter size	Number of kernels	Stride size	Number of weight	Number of bias
Input	1×873	–	–	–	–
Conv-1	1×14	16	(1,5)	224	16
Max-pool	1×4	16	(1,2)	–	–
Conv-2	1×3	32	(1,2)	96	32
Conv-3	1×3	64	(1,1)	192	64
Conv-4	1×3	64	(1,1)	192	64
Conv-5	1×3	64	(1,1)	192	64
DC-1	1×1	–	–	3	1
Softmax	–	–	–	–	–

ground-truth label. The loss function takes the average over the losses for every training sample N, and the training data are the only guide in searching for a possible solution. Here, α and β weigh the importance of physically inconsistent fault detections between the threshold model and the ground truth when minimizing $Loss_{DP}$, respectively, and n denotes the number of health classes (healthy, light damage, and heavy damage); y_{ji}^T denotes the ground truth of the jth sample for the ith health class; and $\overline{y}_{ji}$ denotes the fault detection result of the jth sample for the ith health class by the CNN model.

To embed the physics knowledge into the loss function during neural network training, we employ $Loss_g$ and $Loss_r$ as our physics-informed equations.

$$Loss_g = -\frac{1}{N_g} \sum_{j=1}^{N_g} \sum_{i=1}^{n} y_{ji}^{TM} \log(\overline{y}_{ji}), \qquad (7)$$

$$Loss_r = -\frac{1}{N_r} \sum_{j=1}^{N_r} \sum_{i=1}^{n} y_{ji}^{TM} \log(\overline{y}_{ji}), \qquad (8)$$

Here, $Loss_g$ and $Loss_r$ denote a fault detection penalty for physically inconsistent health classes of healthy and heavy damage, respectively; N_g denotes the number of samples classified by the threshold model as healthy but that the CNN model classified as light or heavy damage; N_r denotes the number of samples that the threshold model classified as heavy damage but the CNN model classified as healthy or light damage; and y_{ji}^{TM} denotes the fault detection result of the jth sample for the ith health class by the threshold model. We highlight the healthy and heavy damage since the physics inconsistency of these two health classes is more likely to cause severe economic losses and safety accidents than that of the health class of light damage. The inconsistent health class of healthy (i.e., false positives) results in unnecessary maintenance that reduces machine utilization, leading to complaints from customers and unnecessary economic expenditure. The inconsistent health class of heavy damage (i.e., false negatives) results in delayed maintenance which in turn may drive the cost of repair up and reduce the life expectancy of machine assets. There is no doubt that the misclassification of light damage can also be costly, but less so than the harm caused by that of healthy and heavy damage. To this end, the customized data-and-physics-driven loss function highlights the physically inconsistent health classes of healthy and heavy damage

from the points of view of economic impacts and model credibility. We expect that the proposed approach will not reduce its accuracy in fault detection due to the misclassification of light damage, and meanwhile, have fewer misclassifications that violated the physical knowledge of bearing fault as much as possible. We test this expectation by comparing the overall fault detection accuracy achieved by the proposed physics-informed deep learning approach to two other deep learning methods equipped with a traditional cross-entropy loss function. The comparison results of this test are presented in Section 5.

During the training process, the physical knowledge regarding fault-relevant information ($Loss_g$ and $Loss_r$) is added to the traditional loss function, $Loss_{all}$. Thus, the customized data-and-physics-driven loss function $Loss_{DP}$ considers the physical information. In some sense, this customized loss function can be understood as an extension to the exclusively data-driven dependent loss function $Loss_{all}$, where $Loss_{all}$ enforces the contribution from the CNN model in minimizing the customized loss function, and $Loss_g$ and $Loss_r$ drive the customized loss function toward the known physical knowledge. With these two additional terms added to the traditional loss function, the proposed approach leverages not only the physical knowledge but also leverages deep learning for bearing fault detection using a neural network architecture.

3.4. Optimization algorithm

Several optimization algorithms can be used to minimize Eq. (5). The stochastic gradient descent algorithm and its variants have been highly successful at training neural networks (Bottou, 2010; Zinkevich et al., 2010). Thus, this study employed stochastic gradient descent with momentum and used a mini-batch size of 128 samples. An initial learning rate of 0.01 was set for all layers and then decreased by a factor of five after every ten training epochs. Table 2 lists several important parameter values used during the training of the physics-informed deep learning model.

The physics-informed deep learning model mainly consists of five convolutional layers and one dense layer. We randomly initialized the weights in each layer according to the Gaussian distribution with a mean of 0 and a standard deviation of 0.01, and the bias values for all the convolutional and dense layers were initialized to 0. The model configurations are outlined in Table 3.

Table 4
Summary of fault sizes.

Fault type	Fault location	Fault size			Severity level	Bearing IDs
		Length (in)	Width (in)	Depth (in)		
Inner race	Outer surface of the inner race	0.4	0.095	0.04	Light damage	1,2
		0.8	0.095	0.08	Heavy damage	3,4
Outer race	Inner surface of the outer race	0.4	0.095	0.04	Light damage	5,6
		0.8	0.095	0.08	Heavy damage	7,8
Roller	Outer surface of the roller	0.6	0.095	0.04	Light damage	9,10
		0.6	0.095	0.08	Heavy damage	11,12

Table 5
Dataset summary.

Dataset	Bearing ID	Number of samples	Condition
Training	13	2235	Healthy
	1	1419	Light damage of inner race
	3	1139	Heavy damage of inner race
	5	3100	Light damage of roller
	7	1238	Heavy damage of roller
	9	3198	Light damage of outer race
	11	3709	Heavy damage of outer race
Test 1	14	2549	Healthy
	2	1192	Light damage of inner race
	4	2181	Heavy damage of inner race
Test 2	15	854	Healthy
	6	1294	Light damage of roller
	8	1288	Heavy damage of roller
Test 3	16	1381	Healthy
	10	2387	Light damage of outer race
	12	766	Heavy damage of outer race
Test 4	17	1358	Healthy
Test 5	18	2880	Healthy

4. Experimental data for Case Study 1

We experimented on an agricultural machine to evaluate the performance of the proposed physics-informed deep learning approach in detecting the faults of roller bearings. The three common types of fault (inner race fault, outer race fault, and roller fault) were introduced as a shallow peck milling slot cut into the bearing components. Fig. 7 shows the outer race of a bearing with a manually introduced fault.

For each fault type, we designed faults with different damage severity levels (light damage and heavy damage). A total of 12 bearings were pretreated according to the fault dimensions specified in Table 4. The pretreated bearings and six untreated (or healthy) bearings were assembled onto hydraulic motors. The motors were run under rotational speeds ranging from 21 Hz to 54 Hz. A vibration sensor was attached to the motor to monitor bearing health conditions. The sampling rate was set to 25,600 Hz to ensure that the Nyquist frequency was higher than the resonance frequency of the machine.

The collected vibration signals were split into a large number of samples; the length of each sample was equal to 25,600, to generate one training dataset and five test datasets. Each test dataset can be used to evaluate the model's performance for certain fault types. The composition of each dataset is shown in Table 5. The variation in rotational speed presents a key challenge of bearing fault detection in real-world scenarios. Fig. 8 shows the rotational speed and the maximum vibration amplitude of the inner race fault sub-band (I_0 in Table 1) for bearing 1 in the training dataset and bearing 2 in the test dataset. The rotational speeds are in the range of 21 to 54 Hz with a stable stage and an unstable stage, leading to a fast time-varying behavior. The fluctuating rotational speed thus makes the vibration data unpredictable but closer to real-world scenarios.

5. Results and discussion

5.1. Case Study 1: fault detection of agricultural machine roller bearings

The fault detection accuracy of the proposed physics-informed deep learning approach was compared with that of a support vector machine (SVM) (Chang and Lin, 2011) and a random forest (RF) (Liaw and Wiener, 2002). The SVM model employed a radial basis function kernel with a regularization parameter of 1. The RF model used 22 trees in the forest and had no limit to the maximum depth of the tree, allowing the nodes to expand up to the point where all leaves were pure (containing less than 1 sample).

To determine the effect of employing the sub-band envelope spectrum and customized data-and-physics-driven loss function, we additionally compared the results of the proposed physics-informed deep learning approach to those of a purely data-driven CNN and a deep learning approach (CNN-S) that considers known physics of bearing faults (i.e., sub-band envelope spectrum). The purely data-driven CNN took the entire envelop spectrum as the input, while the CNN-S took the sub-band envelope spectrum as the input. Both CNN and CNN-S were composed of five convolutional layers and one dense layer and equipped with a traditional cross-entropy loss function to perform bearing health classification.

To minimize the effect of random results caused by the run-to-run variation in training a machine learning model, we generated ten different training and validation datasets and executed each training and validation dataset one time. The mean fault detection results of SVM, RF, CNN, CNN-S, and the physics-informed deep learning approach over the ten runs are shown in Table 6. Table 7 shows a comparison of the results achieved by these five approaches in terms of the best fault detection accuracy out of the ten runs.

Based on these results, we can make the four important observations listed below.

First, the overall fault detection accuracy of the physics-informed deep learning approach is higher than that of CNN, indicating that the proposed physics-informed deep learning approach makes more accurate fault detections than does CNN, which is exclusively data-driven. In other words, these results suggest that incorporating physical knowledge of bearing faults enables more accurate health classifications compared to a method that relies exclusively on sensor data. While the physics-informed deep learning approach performed worse on Test 2 than did the CNN, its overall mean fault detection accuracy (97.27%) was better than that of the CNN (96.94%).

Second, when comparing CNN and CNN-S on Tests 1, 3, 4, and 5, it can be observed that the performance improvements of CNN-S over CNN are attributable to employing the sub-band envelope spectrum. It is not surprising that a purely data-driven deep learning approach cannot effectively discover and leverage information about bearing fault physics that is often hidden in sensor signals. While CNN performed better on Test 2 than that of CNN-S, we highlight the model performance on Tests 3, 4, and 5, as these three tests had not been generated at the time of model development and were thus rigorous tests reflecting the effectiveness of the sub-band envelope spectrum in bearing fault detection.

Fig. 7. A single-point peck milling slot defect on the inner surface of the bearing outer race.
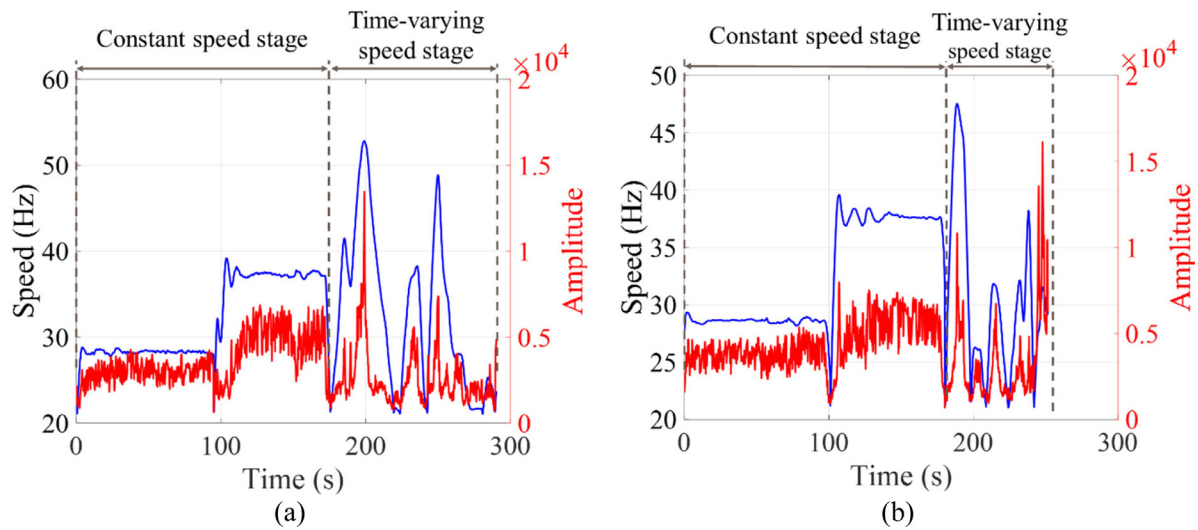

Fig. 8. Speed and vibration amplitude vs. time for (a) bearing 1 in the training dataset and (b) bearing 2 in the test dataset.

Table 6

Mean fault detection results achieved by SVM, RF, CNN, CNN-S, and the physics-informed deep learning approach.

Approach	Input size	Layer	Mean accuracy (%)				
			Test 1	Test 2	Test 3	Test 4	Test 5
SVM	[1,873]	–	93.29	92.28	90.34	98.77	99.63
RF	[1,873]	–	89.32	92.85	82.47	98.78	98.76
CNN	[1,2000]	5 Conv + 1 DC	97.75	97.93	90.40	98.88	99.72
CNN-S	[1,873]	5 Conv + 1 DC	98.74	96.23	91.06	99.15	99.78
Physics-informed deep learning approach	[1,873]	5 Conv + 1 DC	99.19	95.58	92.23	99.38	99.95

Table 7

Best fault detection results achieved by SVM, RF, CNN, CNN-S, and the physics-informed deep learning approach.

Approach	Input size	Layer	Best accuracy (%)				
			Test 1	Test 2	Test 3	Test 4	Test 5
SVM	[1,873]	–	93.54	92.26	91.04	98.89	99.82
RF	[1,873]	–	90.07	92.90	83.17	98.75	98.89
CNN	[1,2000]	5 Conv + 1 DC	98.32	98.52	90.83	99.25	99.77
CNN-S	[1,873]	5 Conv + 1 DC	99.16	97.44	91.18	99.19	99.90
Physics-informed deep learning approach	[1,873]	5 Conv + 1 DC	99.26	96.45	91.82	99.41	99.97

Third, it can be observed that the physics-informed deep learning approach outperformed both CNN and CNN-S on all tests except Test 2, indicating that the data-and-physics-driven loss function leads to more accurate health classifications. The worse performance of the physics-informed deep learning approach on Test 2 may be explained by the distinct difference between the training data and the test data in the vibration amplitude on the envelope spectrum. This difference may bias the fault detection by the threshold model and therefore lead to lower fault detection accuracy of the physics-informed deep learning approach. As our goal is to reduce misclassifications that violate the

Table 8
Confusion matrices for CNN on five test datasets.

Item		Test 1			Test 2			Test 3			Test 4			Test 5		
		True health class														
		🟩	🟨	🟥	🟩	🟨	🟥	🟩	🟨	🟥	🟩	🟨	🟥	🟩	🟨	🟥
Predicted health class	🟩	2515.3	10.9	0.8	837.5	38.2	0.0	1340.8	38.1	0.0	1342.8	0.0	0.0	2871.9	0.0	0.0
	🟨	31.8	1181.1	87.8	16.5	1255.8	16.3	40.2	2060.2	68.4	12.2	0.0	0.0	8.1	0.0	0.0
	🟥	1.9	0.0	2092.4	0.0	0.0	1271.7	0.0	288.7	697.6	3.0	0.0	0.0	0.0	0.0	0.0

Table 9
Confusion matrices for CNN-S on five test datasets.

| Item		Test 1			Test 2			Test 3			Test 4			Test 5		
		True health class														
		🟩	🟨	🟥	🟩	🟨	🟥	🟩	🟨	🟥	🟩	🟨	🟥	🟩	🟨	🟥
Predicted health class	🟩	2516.8	2.1	0.0	842.0	63.6	0.0	1342.6	52.6	0.0	1346.8	0.0	0.0	2874.1	0.0	0.0
	🟨	31.8	1190.3	40.6	12.0	1227.0	50.2	38.8	2026.3	6.3	8.6	0.0	0.0	6.3	0.0	0.0
	🟥	0.0	0.0	2140.2	0.0	3.4	1238.2	0.0	307.7	759.7	3.0	0.0	0.0	0.0	0.0	0.0

Table 10
Confusion matrices for the physics-informed deep learning approach on five test datasets.

Item		Test 1			Test 2			Test 3			Test 4			Test 5		
		True health class														
		🟩	🟨	🟥	🟩	🟨	🟥	🟩	🟨	🟥	🟩	🟨	🟥	🟩	🟨	🟥
Predicted health class	🟩	2541.0	2.4	0.0	850.4	97.8	0.0	1368.0	58.2	0.0	1350	0.0	0.0	2879	0.0	0.0
	🟨	7.6	1190.0	37.8	3.6	1192.0	46.4	13.4	2051.0	3.6	5.4	0.0	0.0	1.4	0.0	0.0
	🟥	0.0	0.0	2143.0	0.0	4.2	1242.0	0.0	277.4	762.4	3.0	0.0	0.0	0.0	0.0	0.0

physical knowledge of bearing faults, the slight accuracy decrease in only one test is not overly concerning. Fourth, the performance (i.e., mean fault detection accuracy) of all three deep learning methods was better than that of SVM and RF. The comparison results suggest that deep neural networks can achieve more accurate fault detection compared to traditional machine learning methods (e.g., SVM and RF).

The results presented in Tables 6 and 7 demonstrate that the physics-informed deep learning approach provides more accurate bearing health class predictions (fewer health class misclassifications) than do the CNN and CNN-S. This performance improvement can be attributed to the use of the data-and-physics-driven loss function, which incorporates the physical knowledge into the CNN model and helps ensure that the health class predictions by CNN are consistent with the known physics of bearing faults.

Fig. 9 shows a box plot that graphically summarizes the numbers of misclassifications that violated the physical knowledge of bearing faults. A misclassification that violates physical knowledge refers to either of the following two cases: (1) a healthy bearing is misclassified as having light or heavy damage while the threshold model classifies it as healthy, and (2) a bearing with heavy damage is misclassified as healthy or having light damage while the threshold model classifies it as having heavy damage. The values of thresholds 1 and 2 were 2800 and 31,000, respectively. These values were empirically determined based on the fault information of the training data as described in Section 3.2. It can be observed from Fig. 9 that (1) the proposed approach (equipped with the data-and-physics-driven loss function) produced smaller total numbers of misclassifications that are inconsistent with the physics as compared to CNN and CNN-S (both are equipped with a traditional loss function) and (2) the number of misclassifications violating the physical knowledge by the physics-informed deep learning approach was less than those of CNN and CNN-S in each test. These comparison results provide evidence that the use of the data-and-physics-driven loss function substantially and consistently reduced the numbers of misclassifications violating physical knowledge.
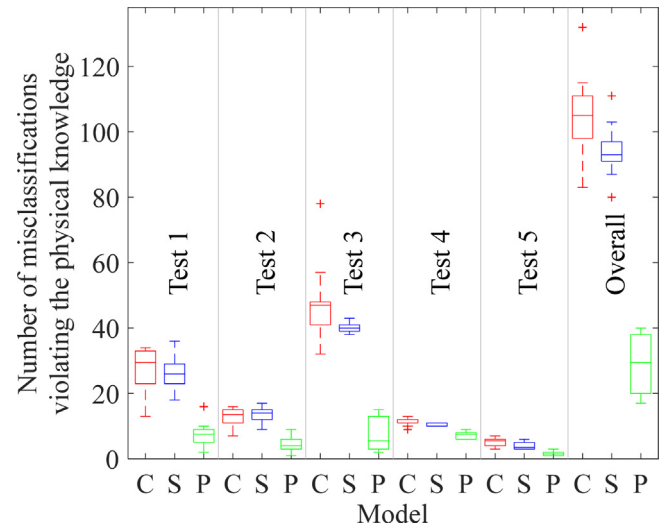
Fig. 9. Comparison of the number of misclassifications that violated the physical knowledge between CNN, CNN-S, and the physics-informed deep learning approach. For simplicity, C, S, and P denote CNN, CNN-S, and the physics-informed deep learning approach, respectively.

5.1.1. Confusion matrix

The results presented in Section 5.1 demonstrate that a deep learning model with embedded physical knowledge can provide more accurate bearing fault detections than can deep learning alone. To explore the underlying reasons, we employed a confusion matrix to visualize the mean fault detection performances of CNN, CNN-S, and the proposed physics-informed deep learning approach on each health class.

A confusion matrix is a visual tool that summarizes the performance of a classification model in bearing fault detection.

The confusion matrices of Tests 1 through 5 achieved by CNN, CNN-S, and the physics-informed deep learning approach are shown in Tables 8 through 10, respectively. The green, yellow, and red squares refer to health classes of healthy, light damage, and heavy damage, respectively. The vertical and horizontal axes represent the predicted bearing health classes and their actual health classes, respectively. More specifically, the elements in the diagonal represent the correct mean fault detections out of ten independent runs, while the elements above and below the diagonal refer to underestimates (i.e., false negatives) and overestimates (i.e., false positives), respectively. Clearly, the physics-informed deep learning approach efficiently reduces the risk of false positives compared to either the purely data-driven CNN approach or the CNN-S approach. Thus, it is reasonable to conclude that the data-and-physics-driven loss function can benefit correct fault detection and reduce the false alarm likelihood. In many real-world applications, this benefit from the appropriate embedding of fault-relevant physical knowledge into the deep learning model is important for reducing maintenance costs, high downtime costs, and customer complaints caused by false positives.

5.1.2. Visualization of deep neural network features

A deep learning-informed approach to bearing fault detection learns the complex fault-relevant features in the envelope spectra of vibration signals. The quality of these features significantly affects fault detection accuracy. However, it is difficult to interpret these features due to their high dimensionality. To understand the implicit meaning of these features and uncover the reasons behind misclassifications, we embedded the high-dimensional features of the last convolutional layer in a two-dimensional space using t-distributed stochastic neighbor embedding (t-SNE). The resulting feature maps for the five tests are shown in Fig. 10. Each sample in a test dataset has input features of sizes 1×2000 (CNN) and 1×873 (CNN-S and the proposed physics-informed deep learning approach). The use of t-SNE allowed visualizing these high-dimensional features in a two-dimensional map. We followed the standard practice for dimensionality reduction. Specifically, principal components analysis was first used to reduce the dimensionality of the features to 40. This first step sped up the computation of pairwise distances between the features and suppressed noise without losing much of the distance information (Maaten and Hinton, 2008). We then used t-SNE to represent the 40-dimensional features in a two-dimensional map that preserved much of the significant relationship of the high-dimensional features.

The following three observations can be made from the plot in Fig. 10. First, when comparing CNN and CNN-S to the proposed physics-informed deep learning approach on Tests 1 through 5, it can be observed that the physics-informed deep learning approach had fewer misclassifications violating the physical knowledge. While CNN-S also considers some known physics of bearing faults (i.e., sub-band envelope spectrum), it is found that this included information was not sufficient to substantially reduce misclassifications violating the physical knowledge. This suggests that the customized data-and-physics-driven loss function, used in the proposed approach, was the main reason for the reduction in misclassifications violating the physical knowledge.

Second, the accurate fault detection results (the overall mean accuracy is 96.94%, 96.99%, and 97.27% for CNN, CNN-S, and the physics-informed deep learning approach, respectively) can be explained by the well-separated health classes as shown in Fig. 10. The clear separations suggest the models were able to identify the boundaries between different classes, and when they were not able to discern a hard boundary, some misclassifications occurred.

Third, a majority of the misclassifications by the physics-informed deep learning approach were located near the boundaries of individual clusters, indicating that these misclassified samples may not possess distinguishable features, which makes it difficult for the approach to correctly determine the health classes.

5.1.3. Effect of the number of layers

It is well known that the performance of a CNN model heavily depends on the number of convolutional layers. We conducted a parametric study to empirically investigate the effect of the number of convolutional layers on the fault detection accuracy and the training time and memory required by the CNN models used in this work. Fig. 11 graphically illustrates the sensitivity of the CNN model to the number of convolutional layers.

The following three observations can be made from Fig. 11.

First, when comparing the model with three convolutional layers to the model with five convolutional layers, the model performance improved sharply as the number of convolutional layers increased. This is not surprising as deeper neural networks can learn more complex functions mapping the input to the output. However, this model performance decreased slightly after the number of convolutional layers exceeded five, indicating that the models with more layers may suffer from overfitting. These results suggest that selecting an inappropriate number of convolutional layers may lead to a decrease in the fault detection accuracy.

Second, the training time and memory increased as the number of convolutional layers increased. This is again expected, as a deeper neural network with a larger number of convolutional layers generally has a larger number of parameters to optimize during training.

Considering the fault detection accuracy and the required training time and memory, the final CNN model used in the proposed physics-informed deep learning approach contained five convolutional layers. The results reported in the other sections of Case Study 1 were produced using this network depth.

5.1.4. Sensitivity to sub-band width

The input to the CNN model consisted of a sample matrix with a fixed size [1,873], corresponding to a 5% sub-band width. To investigate the sensitivity of the CNN model with regard to the input size, we created input matrices of different sizes, including [1,748], [1,817], [1,873], [1,987], and [1,2000], corresponding to 3%, 4%, 5%, and 6% sub-band widths, and the entire envelope spectrum, respectively. Note that when the size of a sample matrix is equal to [1,2000], the entire envelope spectrum is used without any adjustment to the input matrix size. Fig. 12 shows the performances of the CNN models with the various input matrix sizes. Note that all of the considered CNN models consisted of five convolutional layers.

The following three observations can be made from Fig. 12.

First, the CNN models with 4%, 5%, and 6% sub-band widths performed better than the model that took the entire envelope spectrum as the input, indicating that the designed sub-band envelope spectrum enables higher fault detection accuracy. Compared to the model with the input as the entire envelope spectrum, the model that takes the input sub-band envelope spectrum has fewer input features and then emphasizes features closer to the fault characteristic frequencies and their harmonics, which potentially carry more fault-relevant information.

Second, the model performance gradually increased while the sub-band width was less than 5%. This increase can be explained because the higher sub-band widths include more fault-relevant features in the inputs to the CNN model compared to the smaller sub-band widths.

Third, the model with a 6% sub-band width performed worse than the model with a 5% sub-band width. One possible reason is that this width rate included some non-fault-relevant features that might mislead the CNN model. It is also reasonable to consider that including redundant features may reduce the fault detection accuracy.

Considering the overall performance of each considered CNN model, we chose to use a 5% sub-band width in this study, corresponding to an input matrix size of [1,873].
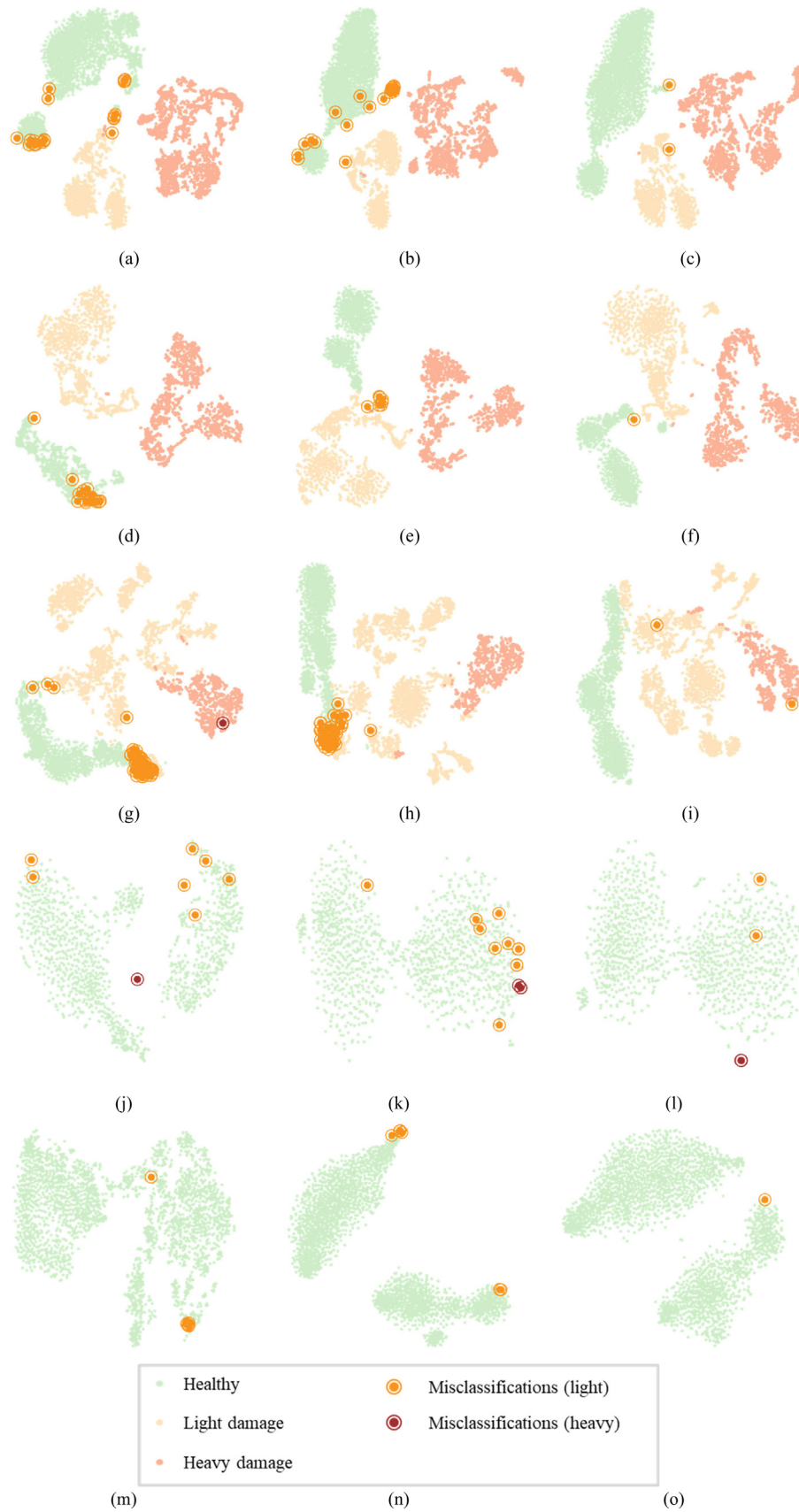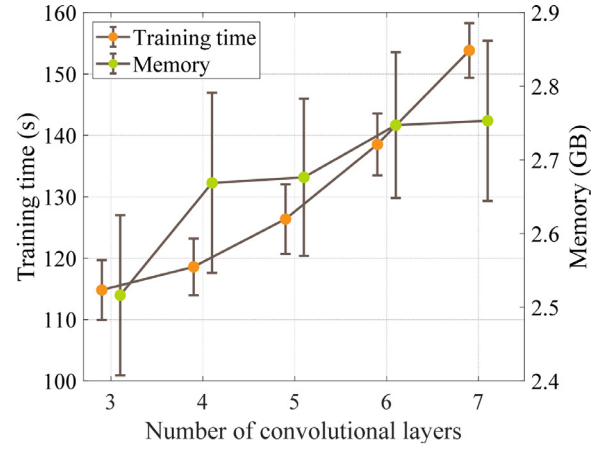
Fig. 10. Visualizations of the learned features by CNN, CNN-S, and the proposed physics-informed deep learning approach using t-SNE on Test 1 (a)–(c), Test 2 (d)–(f), Test 3 (g)–(i), Test 4 (j)–(l), and Test 5 (m)–(o). The features were colored according to the health classes. Note the misclassifications refer to those which violate the physical knowledge.
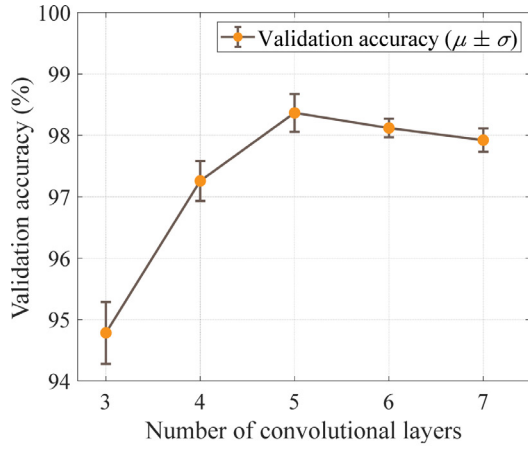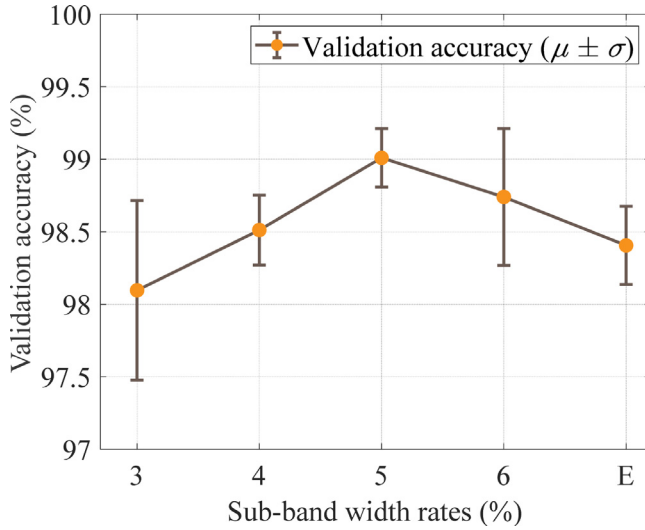
(a)   (b)

Fig. 11. Validation accuracy (a) and training time and memory consumption (b) for a different number of convolutional layers. Ten different training and validation sets were generated to plot the error bars showing the sensitivity of the CNN model to the number of convolutional layers.

Fig. 12. Validation accuracy vs. sub-band widths. Ten different training and validation sets were generated to plot the error bars, which show the effect of the sub-band width (%) on the accuracy of the CNN model. For simplicity, E denotes the entire envelope spectrum without any adjustment to the input matrix size.

Table 11
Comparison of computational time and memory usage on ten different training and validation datasets.

Approach	CNN	CNN-S	Physics-informed deep learning approach
Training time (s)	126.361	101.294	103.924
Test time (s)	0.067	0.045	0.045
Memory (GB)	2.676	2.402	2.404

5.1.5. Computational efficiency

In this subsection, we compare the proposed physics-informed deep learning approach with CNN and CNN-S in terms of computational time and memory usage. This comparison was conducted on an Intel Core i7-8700 CPU @ 3.2 GHz equipped with an NVIDIA Titan Xp GPU with 12 GB GDDR5X memory and 64 GB of system RAM. The Python code used to construct and optimize all the approaches were written by the authors. To minimize the effects of randomness during the measurements, we generated ten different training and validation datasets and executed each on each dataset one time. Table 11 summarizes the mean computational times over the ten runs.

It is not surprising that the training of a CNN model that takes the entire envelope spectrum as the input required more time than did the training of a CNN model with the input sub-band envelope spectrum (CNN-S). Despite the physics-informed deep learning approach consisting of both a CNN and a threshold model, the computational times and memory usage were similar to CNN-S. The similar levels of computational time and memory usages for these two approaches suggest that integrating the threshold model does not incur a heavy computational burden.

5.2. Case Study 2: fault detection of CWRU ball bearings

In this subsection, an open-source dataset from the Case Western Reserve University (CWRU) Bearing Data Center (Loparo) was employed to further investigate the performance of the proposed physics-informed deep learning approach in bearing fault detection. As a standard reference in the bearing diagnostics field, the CWRU dataset has been widely used to evaluate the performance of a machine learning model in bearing condition monitoring and fault detection. The CWRU dataset uses deep groove ball bearings manufactured by SKF and considers three types of bearing faults: inner race faults, outer race faults, and ball faults. An electro-discharge machining (EDM) circular point slot defect was introduced to a bearing using electro-discharge machining. The three sizes of manual faults had diameters of 0.007, 0.014, and 0.021 inches, respectively. The data was collected at both the drive end and fan end, sampled at a frequency of 12 kHz with speeds of 1730, 1750, 1772, and 1797 rpm. Compared with Case Study 1 where the rotational speeds of the bearings were time-varying, the fault detection task for the CWRU dataset is less challenging since the bearings in this dataset were tested at constant speeds.

In this task, we used data collected from seven bearings at the drive end. Among these seven bearings, one was healthy and the other six were faulty (see the fault sizes in Table 12). Each bearing has four vibration signals corresponding to the four speeds. Each vibration signal was split into two sub-signals. The first sub-signal was used to generate training data. Specifically, the sub-signal was subjected to a segmentation process using a fixed-size window of 4096 data points. The second sub-signal went through a similar process to generate test data. The test data was divided into four subsets (i.e., Tests 1, 2, 3, and 4), each at one of the four speeds.

Table 13 summarizes the fault detection accuracy by SVM, RF, CNN, and the proposed physics-informed deep learning approach. The CNN model mainly consisted of five convolutional layers and one dense layer. This network architecture ensured satisfactory accuracy in fault detection. The values of the hyper-parameters used in training SVM,

Table 12
Summary of fault sizes in Case Study 2.

Fault type	Fault location	Fault size		Severity level
		Diameter (in)	Depth (in)	
Inner race	Inner raceway	0.007	0.011	Light damage
		0.021	0.011	Heavy damage
Outer race	Outer raceway	0.007	0.011	Light damage
		0.021	0.011	Heavy damage
Rolling element	Ball	0.007	0.011	Light damage
		0.021	0.011	Heavy damage

Table 13
Fault detection results by SVM, RF, CNN, and the physics-informed deep learning approach on the CWRU dataset.

Approach	Input size	Layer	Accuracy (%)			
			Test 1	Test 2	Test 3	Test 4
SVM	[1,2000]	–	98.50	98.00	100.00	99.91
RF	[1,2000]	–	97.71	97.86	100.00	99.93
CNN	[1,2000]	5 Conv + 1 DC	99.93	99.64	100.00	99.90
Physics-informed deep learning approach	[1,873]	5 Conv + 1 DC	99.64	99.90	99.90	99.90

RF, and CNN were optimized prior to testing. The physics-informed deep learning approach consisted of a deep CNN model and a threshold model. The deep CNN model had the same network architecture as CNN. Thresholds 1 and 2 of the threshold model were 16 and 400, respectively. The model input features (i.e., the vibration amplitudes in the frequency sub-bands in the envelope spectrum) were identified using fault characteristic frequencies $f_{RD} = 4.71$ Hz, $f_{ORD} = 3.58$ Hz, $f_{IRD} = 5.42$ Hz and a 5% sub-band width. The weight factors α and β of the data-and-physics-driven loss function were both set to a constant of 0.05. This setting enabled the physics-informed deep learning approach to produce good accuracy in fault detection. As shown in Table 13, the SVM and RF models achieved exactly or nearly 100% accuracy in tests 3 and 4, and the CNN model and physics-informed deep learning approach achieved exactly or nearly 100% accuracy in all tests. The comparable accuracy between the three existing machine learning approaches (SVM, RF, and CNN) and the proposed physics-informed deep learning approach further verified that the proposed approach was an effective tool for bearing fault detection.

6. Conclusion

In this study, we proposed a physics-informed deep learning approach for bearing fault detection. The proposed approach integrates a simple threshold model and a deep convolutional neural network (CNN) model. The physical knowledge and deep learning methods, both of which are essential to bearing fault detection are intelligently combined through a customized data-and-physics-driven loss function. This loss function incorporates the known physics of bearing faults from the threshold model into the CNN model's training process to address the challenge of physics scarcity in the CNN model. The effectiveness of the proposed physics-informed deep learning approach was verified using data acquired from 18 roller bearings on an agricultural machine operating in the field (Case Study 1) and from ball bearings of the Case Western Reserve University (CWRU) Bearing Data Center (Case Study 2). t-stochastic neighbor embedding (t-SNE) was employed to visualize the features learned by the deep learning models. The visualization offered meaningful insight into the reduction of misclassifications violating physical knowledge. The verification and visualization results demonstrate that the integration of data-driven learning and physics-informed modeling can improve bearing fault detection accuracy and reduce the likelihood of false alarms.

In the two case studies, the proposed physics-informed deep learning approach has shown plausible benefits for bearing fault detection

as compared to two more data-driven approaches. However, these two case studies are limited in the nature of defect geometries, viz. single-point peck milling slot (Case Study 1) and circular point slot (Case Study 2). Our future work will investigate the applicability of the proposed physics-informed deep learning approach to the detection of more minor defects such as cracks that may produce similar characteristic frequencies to those produced by grooves and point defects (Tse et al., 2001; Widodo et al., 2009). This future investigation will allow us to more thoroughly study the effectiveness of the proposed approach in bearing fault detection.

CRediT authorship contribution statement

Sheng Shen: Methodology, Software, Validation, Writing - original draft. **Hao Lu:** Conceptualization, Methodology, Software, Validation, Writing - review & editing. **Mohammadkazem Sadoughi:** Conceptualization, Methodology, Software. **Chao Hu:** Conceptualization, Methodology, Writing - review & editing, Supervision, Project administration. **Venkat Nemani:** Visualization, Writing - review & editing. **Adam Thelen:** Writing - review & editing. **Keith Webster:** Investigation, Data collection. **Matthew Darr:** Investigation, Data collection, Project administration. **Jeff Sidon:** Conceptualization, Resources, Project administration. **Shawn Kenny:** Conceptualization, Resources, Project administration.

Declaration of competing interest

The authors declare that they have no known competing financial interests or personal relationships that could have appeared to influence the work reported in this paper.

Acknowledgments

References

Abboud, D., Elbadaoui, M., Smith, W.A., Randall, R.B., 2019. Advanced bearing diagnostics: A comparative study of two powerful approaches. Mech. Syst. Signal Process. 114, 604–627.

Abdeljaber, O., Avci, O., Kiranyaz, S., Gabbouj, M., Inman, D.J., 2017. Real-time vibration-based structural damage detection using one-dimensional convolutional neural networks. J. Sound Vib. 388, 154–170.

Ahmad, W., Khan, S.A., Kim, J.M., 2017. A hybrid prognostics technique for rolling element bearings using adaptive predictive models. IEEE Trans. Ind. Electron. 65 (2), 1577–1584.

Azamfar, M., Singh, J., Bravo-Imaz, I., Lee, J., 2020. Multisensor data fusion for gearbox fault diagnosis using 2-D convolutional neural network and motor current signature analysis. Mech. Syst. Signal Process. 144, 106861.

Banerjee, T.P., Das, S., 2012. Multi-sensor data fusion using support vector machine for motor fault detection. Inform. Sci. 217, 96–107.

Bottou, Léon, 2010. Large-scale machine learning with stochastic gradient descent. In: Proceedings of COMPSTAT'2010. Physica-Verlag HD, pp. 177–186.

Cai, Baoping, Liu, Hanlin, Xie, Min, 2016a. A real-time fault diagnosis methodology of complex systems using object-oriented Bayesian networks. Mech. Syst. Signal Process. 80, 31–44.

Cai, Baoping, Liu, Yu, Xie, Min, 2016b. A dynamic-Bayesian-network-based fault diagnosis methodology considering transient and intermittent faults. IEEE Trans. Autom. Sci. Eng. 14 (1), 276–285.

Cerrada, M., Sánchez, R.V., Li, C., Pacheco, F., Cabrera, D., de Oliveira, J.V., Vásquez, R.E., 2018. A review on data-driven fault severity assessment in rolling bearings. Mech. Syst. Signal Process. 99, 169–196.

Chang, Chih-Chung, Lin, Chih-Jen, 2011. LIBSVM: A library for support vector machines. ACM Trans. Intell. Syst. Technol. (TIST) 2 (3), 1–27.

Cheng, W., Gao, R.X., Wang, J., Wang, T., Wen, W., Li, J., 2014. Envelope deformation in computed order tracking and error in order analysis. Mech. Syst. Signal Process. 48 (1–2), 92–102.

Cortes, C., Vapnik, V., 1995. Support-vector networks. Mach. Learn. 20 (3), 273–297.

Cover, T., Hart, P., 1967. Nearest neighbor pattern classification. IEEE Trans. Inf. Theory 13 (1), 21–27.

Dolenc, B., Boškoski, P., Juričić, Đ., 2016. Distributed bearing fault diagnosis based on vibration analysis. Mech. Syst. Signal Process. 66, 521–532.

Dou, D., Zhou, S., 2016. Comparison of four direct classification methods for intelligent fault diagnosis of rotating machinery. Appl. Soft Comput. 46, 459–468.

Eren, L., Ince, T., Kiranyaz, S., 2019. A generic intelligent bearing fault diagnosis system using compact adaptive 1D CNN classifier. J. Signal Process. Syst. 91 (2), 179–189.

Feldman, M., 2011. Hilbert transform in vibration analysis. Mech. Syst. Signal Process. 25 (3), 735–802.

Fyfe, K.R., Munck, E.D.S., 1997. Analysis of computed order tracking. Mech. Syst. Signal Process. 11 (2), 187–205.

Glowacz, A., 2019. Fault diagnosis of single-phase induction motor based on acoustic signals. Mech. Syst. Signal Process. 117, 65–80.

Hasan, M.J., Islam, M.M., Kim, J.M., 2019. Acoustic spectral imaging and transfer learning for reliable bearing fault diagnosis under variable speed conditions. Measurement 138, 620–631.

He, X.H., Wang, D., Li, Y.F., Zhou, C.H., 2016. A novel bearing fault diagnosis method based on gaussian restricted boltzmann machine. Math. Probl. Eng. 2016.

Hoang, D.T., Kang, H.J., 2019. A survey on deep learning based bearing fault diagnosis. Neurocomputing 335, 327–335.

Jia, F., Lei, Y., Lin, J., Zhou, X., Lu, N., 2016. Deep neural networks: A promising tool for fault characteristic mining and intelligent diagnosis of rotating machinery with massive data. Mech. Syst. Signal Process. 72, 303–315.

Jin, X., Que, Z., Sun, Y., Guo, Y., Qiao, W., 2019. A data-driven approach for bearing fault prognostics. IEEE Trans. Ind. Appl. 55 (4), 3394–3401.

Jing, L., Zhao, M., Li, P., Xu, X., 2017. A convolutional neural network based feature learning and fault diagnosis method for the condition monitoring of gearbox. Measurement 111, 1–10.

Kang, M., Kim, J., Jeong, I.K., Kim, J.M., Pecht, M., 2016. A massively parallel approach to real-time bearing fault detection using sub-band analysis on an FPGA-based multicore system. IEEE Trans. Ind. Electron. 63 (10), 6325–6335.

Khorram, A., Khalooei, M., 2019. Intelligent bearing fault diagnosis with convolutional long-short-term-memory recurrent neural network. ArXiv preprint arXiv:1909.07801.

Kim, H., Youn, B.D., 2019. A new parameter repurposing method for parameter transfer with small dataset and its application in fault diagnosis of rolling element bearings. IEEE Access 7, 46917–46930.

Lanham, C., 2002. Understanding the Tests that are Recommended for Electric Motor Predictive Maintenance. Baker Instrument Company.

Lei, Y., Jia, F., Lin, J., Xing, S., Ding, S.X., 2016. An intelligent fault diagnosis method using unsupervised feature learning towards mechanical big data. IEEE Trans. Ind. Electron. 63 (5), 3137–3147.

Lei, Y., Yang, B., Jiang, X., Jia, F., Li, N., Nandi, A.K., 2020. Applications of machine learning to machine fault diagnosis: A review and roadmap. Mech. Syst. Signal Process. 138, 106587.

Li, Q., Liang, S.Y., Yang, J., Li, B., 2016. Long range dependence prognostics for bearing vibration intensity chaotic time series. Entropy 18 (1), 23.

Liaw, Andy, Wiener, Matthew, 2002. Classification and regression by randomforest. R News 2 (3), 18–22.

Liu, H., Li, L., Ma, J., 2016. Rolling bearing fault diagnosis based on STFT-deep learning and sound signals. Shock Vib. 2016.

Loparo, K.A., Bearings vibration data set. In: The Case Western Reserve University Bearing Data Center. https://csegroups.case.edu/bearingdatacenter/pages/welcome-case-western-reserve-university-bearing-data-center-website. (Last accessed on 13 April 2021).

Lu, H., Sadoughi, M., Zimmerman, A.T., Hu, C., 2019. Fault diagnosis of rolling element bearings on low-cost and scalable IIoT platform. Struct. Health Monit. 2019.

Lu, C., Wang, Z.Y., Qin, W.L., Ma, J., 2017. Fault diagnosis of rotary machinery components using a stacked denoising autoencoder-based health state identification. Signal Process. 130, 377–388.

Maaten, Laurens van der, Hinton, Geoffrey, 2008. Visualizing data usinrg t-SNE. J. Mach. Learn. Res. 9 (Nov), 2579–2605.

Nandi, S., Toliyat, H.A., Li, X., 2005. Condition monitoring and fault diagnosis of electrical motors—A review. IEEE Trans. Energy Convers. 20 (4), 719–729.

Pan, J., Chen, J., Zi, Y., Li, Y., He, Z., 2016. Mono-component feature extraction for mechanical fault diagnosis using modified empirical wavelet transform via data-driven adaptive Fourier spectrum segment. Mech. Syst. Signal Process. 72, 160–183.

Rai, A., Upadhyay, S.H., 2016. A review on signal processing techniques utilized in the fault diagnosis of rolling element bearings. Tribol. Int. 96, 289–306.

Rai, A., Upadhyay, S.H., 2018. An integrated approach to bearing prognostics based on EEMD-multi feature extraction, Gaussian mixture models and Jensen-Renyi divergence. Appl. Soft Comput. 71, 36–50.

Randall, R.B., Antoni, J., 2011. Rolling element bearing diagnostics—A tutorial. Mech. Syst. Signal Process. 25 (2), 485–520.

Sadeghian, A., Ye, Z., Wu, B., 2009. Online detection of broken rotor bars in induction motors by wavelet packet decomposition and artificial neural networks. IEEE Trans. Instrum. Meas. 58 (7), 2253–2263.

Sadoughi, M., Hu, C., 2019. Physics-based convolutional neural network for fault diagnosis of rolling element bearings. IEEE Sens. J. 19 (11), 4181–4192.

Saufi, S.R., Ahmad, Z.A.B., Leong, M.S., Lim, M.H., 2019. Low-speed bearing fault diagnosis based on ArSSAE model using acoustic emission and vibration signals. IEEE Access 7, 46885–46897.

Schmidhuber, J., 2015. Deep learning in neural networks: An overview. Neural Netw. 61, 85–117.

Seryasat, O.R., Honarvar, F., Rahmani, A., 2010. Multi-fault diagnosis of ball bearing using FFT, wavelet energy entropy mean and root mean square (RMS). In: 2010 IEEE International Conference on Systems, Man and Cybernetics. IEEE, pp. 4295–4299.

Shen, Sheng, Sadoughi, M.K., Chen, Xiangyi, Hong, Mingyi, Hu, Chao, 2018. Online estimation of lithium-ion battery capacity using deep convolutional neural networks. In: ASME 2018 International Design Engineering Technical Conferences and Computers and Information in Engineering Conference. American Society of Mechanical Engineers Digital Collection.

Shen, S., Sadoughi, M., Chen, X., Hong, M., Hu, C., 2019a. A deep learning method for online capacity estimation of lithium-ion batteries. J. Energy Storage 25, 100817.

Shen, Sheng, Sadoughi, Mohammadkazem, Hu, Chao, 2019b. Online estimation of lithium-ion battery capacity using transfer learning. In: 2019 IEEE Transportation Electrification Conference and Expo. ITEC. IEEE, pp. 1–4.

Shen, S., Sadoughi, M., Li, M., Wang, Z., Hu, C., 2020. Deep convolutional neural networks with ensemble learning and transfer learning for capacity estimation of lithium-ion batteries. Appl. Energy 260, 114296.

Sikder, N., Bhakta, K., Nahid, A.Al., Islam, M.M., 2019. Fault diagnosis of motor bearing using ensemble learning algorithm with FFT-based preprocessing. In: 2019 International Conference on Robotics, Electrical and Signal Processing Techniques. ICREST. IEEE, pp. 564–569.

Singh, S., Kumar, N., 2016. Detection of bearing faults in mechanical systems using stator current monitoring. IEEE Trans. Ind. Inf. 13 (3), 1341–1349.

Soualhi, M., Nguyen, K.T., Soualhi, A., Medjaher, K., Hemsas, K.E., 2019. Health monitoring of bearing and gear faults by using a new health indicator extracted from current signals. Measurement 141, 37–51.

Tang, B., Liu, W., Song, T., 2010. Wind turbine fault diagnosis based on Morlet wavelet transformation and Wigner-Ville distribution. Renew. Energy 35 (12), 2862–2866.

Tian, J., Morillo, C., Azarian, M.H., Pecht, M., 2015. Motor bearing fault detection using spectral kurtosis-based feature extraction coupled with K-nearest neighbor distance analysis. IEEE Trans. Ind. Electron. 63 (3), 1793–1803.

Tsao, Ta-Peng, Wu, Rofig-Ching, Ning, Chia-Ching, 2001. The optimization of spectral analysis for signal harmonics. IEEE Trans. Power Deliv. 16 (2), 149–153.

Tse, P.W., Peng, Y.A., Yam, R., 2001. Wavelet analysis and envelope detection for rolling element bearing fault diagnosis—their effectiveness and flexibilities. J. Vib. Acoust. 123 (3), 303–310.

Van Hecke, B., Yoon, J., He, D., 2016. Low speed bearing fault diagnosis using acoustic emission sensors. Appl. Acoust. 105, 35–44.

Vincent, P., Larochelle, H., Lajoie, I., Bengio, Y., Manzagol, P.A., 2010. Stacked denoising autoencoders: Learning useful representations in a deep network with a local denoising criterion. J. Mach. Learn. Res. 11 (Dec), 3371–3408.

Wang, Y., Xiang, J., Markert, R., Liang, M., 2016. Spectral kurtosis for fault detection, diagnosis and prognostics of rotating machines: A review with applications. Mech. Syst. Signal Process. 66, 679–698.

Wang, Y., Xu, G., Liang, L., Jiang, K., 2015. Detection of weak transient signals based on wavelet packet transform and manifold learning for rolling element bearing fault diagnosis. Mech. Syst. Signal Process. 54, 259–276.

Widodo, Achmad, Kim, Eric Y., Son, Jong-Duk, Yang, Bo-Suk, Tan, Andy C.C., Gu, Dong-Sik, Choi, Byeong-Keun, Mathew, Joseph, 2009. Fault diagnosis of low speed bearing based on relevance vector machine and support vector machine. Expert Syst. Appl. 36 (3), 7252–7261.

Xing, S., Lei, Y., Jia, F., Lin, J., 2017. Intelligent fault diagnosis of rotating machinery using locally connected restricted Boltzmann machine in big data era. In: 2017 IEEE International Conference on Industrial Engineering and Engineering Management. IEEM. IEEE.

Zhang, W., Li, C., Peng, G., Chen, Y., Zhang, Z., 2018. A deep convolutional neural network with new training methods for bearing fault diagnosis under noisy environment and different working load. Mech. Syst. Signal Process. 100, 439–453.

Zhang, W., Peng, G., Li, C., Chen, Y., Zhang, Z., 2017. A new deep learning model for fault diagnosis with good anti-noise and domain adaptation ability on raw vibration signals. Sensors 17 (2), 425.

Zhao, R., Yan, R., Chen, Z., Mao, K., Wang, P., Gao, R.X., 2019. Deep learning and its applications to machine health monitoring. Mech. Syst. Signal Process. 115, 213–237.

Zinkevich, Martin, Weimer, Markus, Li, Lihong, Smola, Alex J., 2010. Parallelized stochastic gradient descent. In: Advances in Neural Information Processing Systems. pp. 2595–2603.